

The MECO experiment: A search for lepton flavor violation in muonic atoms

James L. Popp for the MECO Collaboration

Department of Physics, New York University, New York, NY 10003

Abstract

MECO will search for direct evidence of muon and electron flavor violation in the decay of muons in Coulomb bound states via coherent recoil of the nucleus and decay electron. The expected sensitivity to the $\mu^-N \rightarrow e^- + N$ branching fraction relative to muon capture $\mu^-N(A, Z) \rightarrow \nu_\mu + N(A, Z - 1)$ is $R_{\mu e} < 5 \times 10^{-17}$ at 90% confidence level, roughly three to four orders of magnitude lower than current limits. This article provides an overview of the experiment.

1 Introduction

Lepton-flavor-violating transition searches are likely to be sensitive probes of super-unified theories since the predicted rates are often nearest experimental limits. Although precise predictions of theories depend on the specific model, the physical mechanisms that lead to lepton flavor violations are generic to supersymmetric quark-lepton unification. Many extensions to the Standard Model that unify quarks and leptons, including supersymmetric theories, e.g., [1], suggest that in muonic atoms the branching fraction for coherent conversion of a muon into an electron relative to muon capture in the nucleus $R_{\mu e} \sim 10^{-14} - 10^{-17}$ over much of the parameter space. In terms of decay rates, with mass number A and atomic number Z , $R_{\mu e} = \Gamma(\mu^-N(A, Z) \rightarrow$

$e^- + N(A, Z))/\Gamma(\mu^-N(A, Z) \rightarrow \nu_\mu + N(A, Z - 1))$, where the numerator only involves the internal nuclear ground state and denominator includes all possible nuclear final states. The MECO experiment [2] will search for direct evidence for this lepton-flavor-violating process.

The signature of coherent muon-electron conversion is a two-body final state with a mono-energetic E_o electron. When the internal state of the nucleus remains in the ground state during the transition the electron recoils coherently off the entire nucleus, resulting in a strong enhancement in the conversion rate. The electron energy $E_o \simeq E_\mu + E_\mu^2/2M_N$ with $E_\mu = m_\mu + \text{BE}$, the muon mass plus Coulomb binding energy BE. The Schrödinger equation gives good estimates of BE for light nuclei; neglecting the size of the nucleus in alu-

minum, the MECO stopping target material, $BE(1s) \sim -0.48 \text{ MeV}$ and $E_o \sim 105.0 \text{ MeV}$. MECO will look for conversion electrons in the energy window $103.6\text{-}105.1 \text{ MeV}$, where the signal to background ratio is ~ 20 .

The dominant background as in previous experiments [3,4] is muon decay in orbit $\mu^- N \rightarrow \nu_\mu + \bar{\nu}_e + e^- + N$; the electron energy spectrum falls rapidly near the endpoint at exactly the conversion energy, $\propto (E_o - E_e)^5$. Thus background rejection improves rapidly with energy resolution. The MECO tracker probes this crucial region more deeply than ever before.

The current measured limit set by Sindrum II [3] is $R_{\mu e} < 6.1 \times 10^{-13}$ at 90% confidence in titanium, with sensitivity expected to improve soon to 2×10^{-14} . This experiment is limited by beam intensity, not background. With a significantly scaled-up approach to muon production and transport, $\sim 1.8 \times 10^{11} \mu^-/\text{s}$ at the stopping target and at least 10^4 greater than existing low-energy ($p < 100 \text{ MeV}/c$) muon beams, MECO is expected to improve on these limits by at least three to four orders of magnitude $R_{\mu e} < 5 \times 10^{-17}$.

2 The experiment

The MECO setup is shown in Figure 1 and consists of three large superconducting magnets: the muon production, transport, and detector solenoids. The clear bores of the magnets are connected forming a single cavity, held in vacuum. The magnetic field is continuous throughout the cavity. In the 4 m long production solenoid, the axial magnetic

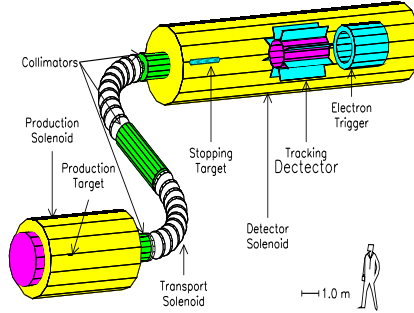


Fig. 1. The MECO experiment

field intensity B is graded from 3.6 T to 2.3 T. The field follows the 12 m S-shaped transport solenoid, falling only in the straight sections from 2.3 T to 2.0 T. In the 10.5 m detector solenoid B is graded from 2.0 T at the entrance to 1.0 T between the stopping target and tracking detector, and constant thereafter. Both the trigger and tracker are high-rate detectors with their detection material positioned far from the solenoid axis to intercept conversion electron helices and avoid beam particle interactions.

The primary proton beam is provided by the Alternating Gradient Synchrotron (AGS), with ~ 1 sec machine cycle for 40×10^{12} protons. The choice of beam energy, 7-8 GeV, optimizes π and minimizes \bar{p} (a potential background source) production. The beam (not shown) enters the production solenoid on the right at 10° to the axis and exits to the left. A tungsten target is bombarded to produce π^\pm which subsequently decay to μ^\pm , following helical trajectories along the magnet axis. The graded field reflects left-moving charged particles with momenta outside the 30° (half angle) loss cone, toward the transport entrance. Since particle energy and

p_{\perp}^2/B are constant, as charges move to regions of lower B the angle χ between the momentum and solenoid axis decreases. Pions with transverse momenta $p_{\perp} < 180 \text{ MeV}/c$ travel within the 30 cm inner radius of the magnet. Most π decays occur in the production region.

A pulsed beam with good extinction ε between pulses is critical to prompt background rejection and thus success for MECO. The mean lifetime for μ^- in aluminum atoms $\tau_{\mu}^{\text{Al}} = 880 \text{ ns}$ sets the pulse separation time scale. Thus the pulse spacing is microseconds and given by $\tau_{\text{pulse}} + \tau_{\text{delay}} + \tau_{\text{obs}}$. The actual proton pulse time $\tau_{\text{pulse}} \ll \tau_{\mu}^{\text{Al}}$. Prompt backgrounds are reduced to an acceptable level by, first, introducing a delay τ_{delay} between each proton pulse and the detection window τ_{obs} so that all beam particles have left the detector region before τ_{obs} ; and second, by requiring that the ratio of protons crossing the production target during the observation window to that during the pulse be $\varepsilon \sim 10^{-9}$. AGS extinction studies are ongoing with current measured value $\varepsilon \sim 10^{-7}$.

The transport solenoid filters the particle flux producing a momentum- and charge-selected muon beam, with good reduction in contamination from e^{\pm} , μ^+ , π^{\pm} , p , and \bar{p} . Transport entrance and exit collimators with 15 cm inner radius further limit the beam. For sufficiently low momenta, centers of particle orbits follow the S-shape of the solenoid; however, the curvature of the magnetic field in the two bent sections gives rise to a drift out of the plane of the magnet. In the first section pos-

itives drift up and negatives down, and in the second directions are reversed. By vertically limiting the aperture of a narrower collimator in the center straight section with a downward offset positives and high-energy negatives are absorbed from the beam. Low-energy antiprotons originating in the production region have long transport crossing times, and as already mentioned the potential to create backgrounds at the detectors. A thin beryllium window in the center section reduces the \bar{p} component to a negligible level. The shallow grades in B in each straight section further prevents late arrivals. At the transport exit e^+ and μ^+ have $p < 40 \text{ MeV}/c$, most e^- have $p < 80 \text{ MeV}/c$ with none above $100 \text{ MeV}/c$. The μ^- beam has $14 \text{ MeV}/c < p < 100 \text{ MeV}/c$.

Only μ^- below $50 \text{ MeV}/c$ stop in the target. Negative muons come to rest in matter by slowing to thermal-like velocities through inelastic atomic collisions and falling into a Coulomb orbit about a nucleus. Excited states cascade to lower ones with time scale 10^{-13} s producing X-rays and Auger electrons. Approximately 60% are captured by the nucleus and 40% decay in orbit.

The stopping target design optimizes the probability for muon stopping and conversion electron detection, and minimizes energy loss of exiting signal e^- and the number of decay-in-orbit electrons reaching the detectors. Background rates are reduced by minimizing stopping target mass. The target has 17 parallel disks 0.02 cm thick with 5.0 cm spacing and radii from 8.3-6.5 cm; total mass is 159 g. Simulations yield a stopping

efficiency $0.0025 \mu^-$ per proton, i.e., 10^{11} Hz stop rate.

The target is centered in the graded field between 1.63-1.37 T; the gradient reflects e^- emitted upstream back to the detectors, resulting in $\sim 60\%$ of all conversions hitting the tracker. Conversion electrons with $p_{\perp} > 90 \text{ MeV}/c$ ($120^\circ > \chi > 60^\circ$) are swept forward by the decreasing magnetic field into the range $75 \text{ MeV}/c < p_{\perp} < 90 \text{ MeV}/c$ ($45^\circ < \chi < 60^\circ$) at the tracking detector. Beam particles with $p_{\perp} < 90 \text{ MeV}/c$ that do not scatter in the target pass down the center of the solenoid without intercepting the detectors. Placing the target in a graded field also ensures that e^- originating upstream of the gradient with $105 \text{ MeV}/c$ arrives at the detectors with $p_{\perp} < 75 \text{ MeV}/c$, eliminating many potential backgrounds. On average the stopping target produces $2n$, 2γ , and $0.1p$ per muon capture, displacing the detectors $> 1 \text{ m}$ downstream from the target greatly reduces acceptance for n and γ .

The straw tube drift chamber tracking detector has large acceptance for and measures with good efficiency the helix parameters of conversion electrons in the uniform field. Good energy resolution is essential to distinguish conversion electrons from decay in orbit, $\lesssim 900 \text{ keV}$ FWHM. Resolution is dominated by scattering in the tracker, and to a much lesser extent by pattern recognition errors. Energy loss in the target, proton absorbers (not shown), and tracker broadens the peak of the resolution function for conversions, and introduces a small mean energy loss and low-energy tail.

The tracker has 16 rectangular planes, 8 forming an octagon centered on the solenoid axis and 8 positioned at each corner extending radially. This geometry gives ≥ 3 plane crossings per conversion e^- helix orbit; 3 m long detector planes guarantee ≥ 2 helix orbits in the detector, a powerful advantage for pattern recognition. With tubes parallel to the length of a plane, a slight tilt of each plane, $< 1^\circ$, prevents a conversion e^- from entering the same tube on different orbits.

Each plane has three layers of 0.25 cm radius circular tubes in a close-packed arrangement; each tube contains a central anode wire. Drift time information and wire positions combine to give the track-detector plane crossing position perpendicular to the wires and the track projection angle (valuable for pattern recognition) in a plane perpendicular to the wires and wire planes. Position along the wires is measured with capacitively-coupled cathode foils, $\sim 1 \text{ cm}$ wide, running perpendicular to the wires on both sides of a plane. Resolutions from wire information are highly angle-dependent with average position and angle resolutions, expressed as root mean square (RMS) quantities, 0.014 cm and 1.0° . The expected RMS pad resolution is $\sim 0.05 \text{ cm}$.

The purpose of the trigger calorimeter is to select with high efficiency conversion electrons that pass through the tracker, while minimizing triggers from lower-energy events. A high degree of segmentation limits signal pile-up. Since background rises exponentially as the trigger threshold decreases, it is

important to have $E_{\text{threshold}}$ as high as possible. The calorimeter should also have good energy and position resolution to provide an independent measurement of these quantities for the helix, a feature shown to have high discriminant value to suppress background.

Trigger design is currently under development. The current design (not shown) using single $3 \times 3 \times 12 \text{ cm}^3$ crystals of BGO (300 ns EM shower decay constant) and avalanche photodiodes show that $E_{\text{threshold}} = 80 \text{ MeV}$ gives 87% efficiency for conversions. This results in an acceptable 0.2 kHz trigger rate. The RMS position and energy resolutions for 105.0 MeV electrons are 1.0 cm and 5.3 MeV. Research continues on other materials with shorter decay times, such as GSO and PbWO_4 .

A conversion electron candidate event has: (1) detector signals within the observation time window, (2) calorimeter shower energy $\geq E_{\text{threshold}}$, (3) detector plane crossings found by pattern recognition consistent with a helix of ≥ 2 helix orbits, (4) a helix which when extended back intersects the stopping target and extended forward is consistent with the calorimeter shower position, (5) p_{\perp} of the helix in the range $75 \text{ MeV}/c < p_{\perp} < 90 \text{ MeV}/c$, (6) helix energy consistent with calorimeter shower energy, and (7) helix energy between 103.6-105.1 MeV.

3 Conclusion

Table 1 summarizes calculations of primary background contributions in the energy window 103.6-

Source	Events
μ^- DIO	0.25
Pattern Recognition	< 0.006
μ^- RC	< 0.005
★ μ^- DIF (a)	< 0.03
★ μ^- DIF (b)	0.04
★ π^- RC	0.07
★ π^- DIF	< 0.001
★ beam e^-	< 0.04
π^- RC	0.001
\bar{p} induced	0.007
CR induced	0.004
Total	< 0.45

Table 1

Expected MECO backgrounds (abbreviations in text) for $\varepsilon = 10^{-9}$ and 10^7 s running time. Stars indicate extinction dependence.

105.1 MeV for a running time of one-third of a year. Decay in orbit (DIO) and radiative capture (RC) of μ^- are intrinsic to muon decay, both are made negligible with precise energy measurement. Starred entries arise from out-of-time proton crossings at the production target which are proportional to the extinction: Decay in flight (DIF) of μ^- without (a) and with (b) scattering in the stopping target, radiative pion capture, DIF for π^- , and beam e^- . The next two backgrounds in the table are from source particles with long transit times in the transport solenoid. Acceptable cosmic ray (CR) induced background rejection for MECO requires passive and active shielding with a modest improvement over previous [3,4]. Inefficiency in the CR

Running time (s)	10^7
Protons/s	4×10^{13}
μ^- stopped /p	0.0025
$P(\mu^- \text{ capture})$	0.60
$F(\tau_{\text{obs}}, \mu^- \text{ capture})$	0.49
Trigger efficiency	0.90
Fitting/selection	0.19
$R_{\mu e}$	10^{-16}
Detected events	5

Table 2
Expected MECO sensitivity.

shield veto is expected to be 10^{-4} . Assuming $\varepsilon \sim 10^{-9}$ the total number of background events expected is < 0.45 .

Table 2 shows that a four-month run and $R_{\mu e} = 10^{-16}$ yields ~ 5 muon-electron conversion events. The number of muon captures is just the product of the first seven entries of Table 2, where $P(\mu^- \text{ capture})$ is the probability of μ^- capture, $F(\tau_{\text{obs}}, \mu^- \text{ capture})$ the fraction of μ^- capture in the observation window, and the overall fitting and event selection criteria efficiency is given.

References

- [1] R. Barbieri, L. Hall, Phys. Lett. B 338 (1994) 212; R. Barbieri, L. Hall, and A. Strumia, Nucl. Phys. B 445 (1995) 219.
- [2] MECO Collaboration, Rare Symmetry Violating Processes 'RSVP': A Proposal to the National Science Foundation to Construct the MECO and KOPIO Experiments, (1999), <http://meco.ps.uci.edu/>.
- [3] Sindrum II Collaboration, Proc. of 6th Conference on Intersections of Particle and Nuclear Physics, T. Donnelly, ed. (AIP, New York, 1997), p.34; C. Dohmen et al., Phys. Lett. B 317 (1993) 631.
- [4] S. Ahmad et al., Phys. Rev. D 38 (1988) 2102.